Available online at www.sciencedirect.com
ScienceDirect
Comparative Biochemistry and Physiology, Part C 145 (2007) 15–27
CBP
www.elsevier.com/locate/cbpc

Microarray analysis identifies keratin loci as sensitive biomarkers for thyroid hormone disruption in the salamander *Ambystoma mexicanum*☆

Robert B. Page [a,1], James R. Monaghan [a,1], Amy K. Samuels [a], Jeramiah J. Smith [a], Christopher K. Beachy [b], S. Randal Voss [a,*]

[a] *Department of Biology and Spinal Cord and Brain Injury Research Center, University of Kentucky, Lexington, KY 40506, United States*
[b] *Department of Biology, Minot State University, Minot, ND 58707, United States*

Received 6 February 2006; received in revised form 17 June 2006; accepted 19 June 2006
Available online 22 June 2006

Abstract

Ambystomatid salamanders offer several advantages for endocrine disruption research, including genomic and bioinformatics resources, an accessible laboratory model (*Ambystoma mexicanum*), and natural lineages that are broadly distributed among North American habitats. We used microarray analysis to measure the relative abundance of transcripts isolated from *A. mexicanum* epidermis (skin) after exogenous application of thyroid hormone (TH). Only one gene had a >2-fold change in transcript abundance after 2 days of TH treatment. However, hundreds of genes showed significantly different transcript levels at days 12 and 28 in comparison to day 0. A list of 123 TH-responsive genes was identified using statistical, BLAST, and fold level criteria. Cluster analysis identified two groups of genes with similar transcription patterns: up-regulated versus down-regulated. Most notably, several keratins exhibited dramatic (1000 fold) increases or decreases in transcript abundance. Keratin gene expression changes coincided with morphological remodeling of epithelial tissues. This suggests that keratin loci can be developed as sensitive biomarkers to assay temporal disruptions of larval-to-adult gene expression programs. Our study has identified the first collection of loci that are regulated during TH-induced metamorphosis in a salamander, thus setting the stage for future investigations of TH disruption in the Mexican axolotl and other salamanders of the genus *Ambystoma*.

Keywords: Ambystoma; Mexican axolotl; Microarray; Endocrine disruption; Thyroid hormone; Metamorphosis; Keratin; RT-PCR

1. Introduction

Vertebrates use many of the same hormones to regulate periods of post-embryonic development. For example, thyroid hormone (TH) is essential for initiating and orchestrating amphibian metamorphosis, a developmental period in which a suite of genetic, molecular, cellular, morphological, and physiological changes are induced to transform aquatic larvae into more terrestrial adults. Similarly, TH is essential for initiating normal growth and maturation of organ systems during critical windows of early mammalian development. Many aspects of TH regulation and action are evolutionarily conserved between mammals and amphibians, including thyroid hormone synthesis, secretion, and transport (Barrington, 1962; Larsson et al., 1985; Power et al., 2000), tissue-specific regulation of TH concentration (St. Germain and Galton, 1997; Kester et al., 2004), attenuation of TH affect via synergistic interactions with corticosteroids (Hayes, 1997; Helmreich et al., 2005; Kuhn et al., 2005), TH-mediated regulation of gene expression by steroid nuclear receptor isoforms and accessory factors (Lazar, 1993; Brent, 1994; Shi, 2000; Buchholz et al., 2006), and pituitary regulation of TH release (Denver et al., 2002). The conservation of TH-dependent development among vertebrates indicates that tractable non-mammalian organisms can be exploited as models for TH disruption in human.

☆ This paper is based on a presentation given at the conference: *Aquatic Animal Models of Human Disease* hosted by the University of Georgia in Athens, Georgia, USA, October 30–November 2, 2005.

* Corresponding author. Tel.: +1 859 257 9888; fax: +1 859 257 1717.
E-mail address: srvoss@uky.edu (S.R. Voss).

[1] Co-first authors.

1532-0456/$ - see front matter © 2006 Elsevier Inc. All rights reserved.
doi:10.1016/j.cbpc.2006.06.003

Amphibians offer special advantages for studying endocrine disruption of TH and other developmentally important hormones (Tata, 1993). In contrast to working with early mammalian life stages, it is straightforward to administer hormones to free-living amphibian embryos and larvae to study the effects of normal and disrupted endocrine signaling on development (e.g. Kitamura et al., 2005). Hormones and toxicants can simply be added to the water in which amphibians are housed and developmental effects can be measured using either gross morphology (e.g. Degitz et al., 2005) or molecular tools (e.g. Turque et al., 2005). Another advantage is that the amphibian metamorphic program presents some of the same basic questions that confront researchers working on early mammalian development (e.g. Zoeller, 2004): *How does a single molecule (TH) orchestrate different cellular-level changes and coordinate developmental processes among multiple tissue types*, and *What are the consequences of delayed or inadequate delivery of TH during critical windows of development*? Indeed, the recent finding that a single quantitative trait locus contributes to both developmental timing variation and clinical hypothyroidism in a non-metamorphosing salamander suggests there is much to be learned from studying amphibians (Voss and Smith, 2005). Over the last few decades, amphibian research has helped conceptualize TH-associated trade-offs in allocations to growth, maturation, and developmental plasticity. This body of work is providing a framework for understanding the consequences of disrupted, fetal and natal development in humans (Amiel-Tison et al., 2004; Crespi and Denver, 2004; Zoeller, 2004).

In addition, amphibians are likely to become important sentinels in determining minimal contaminate levels that threaten human health. Natural populations of amphibians are declining rapidly and there is growing concern that endocrine disrupting chemicals are contributing significantly to their demise (e.g. Reeder et al., 2005). For example, the herbicide Atrazine has been linked to developmental abnormalities, reduced growth, and altered metamorphic timing (Hayes, 2005); such insults can affect larval life history parameters (e.g., age and size at metamorphosis, and future reproductive success) that directly impact long-term population stability (sensu Semlitsch et al., 1988; Wilbur, 1996). To better monitor natural populations for endocrine disruption, it will be important to develop methods that allow comprehensive assessment of the thyroidal axis, from neuroendocrine control to target tissues. Additionally, methods must be able to diagnose TH axis disruptions of development from a multitude of natural and anthropomorphic stressors that can yield convergent phenotypes at the morphological level.

Microarray analysis offers the potential to identify diagnostic gene expression patterns that can differentiate among different types of endocrine disruption. Microarray analysis may also provide the power to differentiate among the several molecular and cellular bases (i.e. sites of action) that are possible for each disrupter type. To date, relatively few microarray resources have been developed and applied for work in amphibians, with all effort directed toward anurans (Crump et al., 2002; Baldessari et al., 2005; Chalmers et al., 2005; Turque et al., 2005). We developed a custom Affymetrix GeneChip to identify and monitor genes that are responsive to TH signaling and endocrine disruption in *Ambystoma mexicanum*, a salamander with a maturing, model organism infrastructure. Genomic, bioinformatic, and living stock resources are available for ambystomatids and a networking infrastructure is under development (Smith et al., 2005). Ambystomatids are easily reared in the laboratory using standardized culture methods and they offer the advantage of being broadly distributed among North American habitats. We report the results of a study that measured the relative abundance of transcripts isolated from Mexican axolotl (*A. mexicanum*) epidermis (skin) after exogenous application of TH to whole animals. Our study has identified the first collection of loci that are regulated during TH-induced metamorphosis in a salamander amphibian, and thus set the stage for future investigations of TH disruption in the axolotl and other ambystomatid salamanders.

2. Methods and materials

2.1. Salamanders, experimental design, and tissue collection

Salamanders (*A. mexicanum*) were obtained from a single genetic cross, using adults from an inbred strain that is maintained by Voss's group at the University of Kentucky. Embryos and larvae were reared individually at 20–22 °C in 40% Holtfreter's solution. After hatching, larvae were fed freshly hatched brine shrimp (*Artemia* sp.) nauplii until they were large enough (3 weeks) to eat California blackworms (*Lumbriculus* sp.; J.F. Enterprises). At approximately 8 months of age, 24 animals were randomly assigned to the T4 treatment group. Individuals in the T4 treatment group were reared in 40% Holtfreter's containing 50 nM tetraiodothyronine (T4, Sigma). A stock solution of 100 μM T4 was made by first dissolving 100 mg T4 (Sigma T2376) in 1 mL of 1.0 M NaOH and then adjusting the volume of this solution to 10 mL with 0.4 M NaOH. Five milliliters of this solution was then added to 645 mL sterile-distilled water to obtain a 100 μM stock. 50 nM T4 was made fresh daily by mixing 25 mL of T4 100 μM stock with 40% Holtfreter's solution to a final volume of 50 l. Water was changed daily during the experiment. Skin tissue was collected from eight untreated salamanders on day 0 of the experiment and eight treated salamanders at each of three time points: following 2, 12, and 28 days of chronic exposure to T4. These time points were sampled to test for early gene expression changes that might precede morphological metamorphosis, and because 28 days is a sufficient period for complete metamorphosis of TH-induced *A. mexicanum*. To obtain tissue, salamanders were anesthetized in 0.01% Benzocaine (Sigma) and a ~1 cm^2 piece of skin tissue was removed from the top of the head. Gross phenotypic changes associated with T4 treatment of axolotls included resorption of external gills and loss of upper and lower larval tail fins. We used a 4 stage developmental series (Cano-Martinez et al., 1994) to describe morphological changes after TH-induced metamorphosis in *A. mexicanum*.

2.2. Ambystoma GeneChip

A custom Ambystoma Affymetrix GeneChip was designed from curated EST assemblies for the species *A. mexicanum* and *A. t. tigrinum* that are available from the Ambystoma EST Database (http://salamander.uky.edu/ESTdb; Smith et al., 2005). The Amby_001 array is tiled in a 100–3660 format with 11 μm features. Probe sets were designed using a preferred maximum of 11 probe pairs (match/mismatch) and a possible minimum of 8 probe pairs. Only 8 probe sets on the GeneChip contain fewer than 11 probe pairs. The GeneChip contains 4844 total probe sets, 254 of which are controls or replicate probe sets. The remaining 4590 probe sets correspond to unique *A. mexicanum* or *A. tigrinum* contigs, of which 2960 are significantly identical in nucleotide composition (e−7; BLASTX) to a human sequence in the non-redundant, RefSeq protein database.

2.3. RNA isolation, probe preparation, and microarray hybridization

Total RNA was extracted for each independent tissue sample with TRIzol (Invitrogen) according to the manufacturer's protocol; additionally, RNA preparations were further purified using a Qiagen RNeasy mini column (Qiagen). UV spectrophotometry and a 2100 Agilent Bioanalyzer (Agilent Technologies) were used to quantify and qualify RNA preparations. Three high quality RNA isolations from each time point (days 0, 2, 12, 28) were used to make three individual-specific, pools of biotin labeled cRNA probes. Each of the 12 pools was subsequently hybridized to an independent GeneChip. The University of Kentucky Microarray Core Facility generated cRNA probes and performed hybridizations according to standard Affymetrix protocols.

2.4. Data analysis

Background subtraction, normalization, and data transformation were performed using the Robust Multiple-array Average (RMA) algorithm (Irizarry et al., 2003). Analysis of variance (ANOVA) was used, independently for each probe set to test for significant differences in hybridization intensity across the four sampling times (day 0, day 2, day 12, and day 28). ANOVA was performed using $\log_2$ transformed data via J/MAANOVA software (Wu and Churchill, 2005) and the gene specific *F*-test (F_1) described by Cui and Churchill (2003). We controlled the False Discovery Rate (FDR) using a step-up algorithm to give a FDR threshold of 0.001 (Benjamini and Hochberg, 1995; Reiner et al., 2003). Hybridization intensities were averaged across each of the replicate GeneChips within the control and T4-treated groups for all further analyses.

Genesis, Version 1.6.0 Beta 1 software (Sturn, 2000; Sturn et al., 2002) was subsequently used to cluster a candidate list of 123 genes into discrete categories based on their expression patterns. This clustering was conducted on $\log_2$-ratio data and was accomplished by implementing a Self Organizing Map (SOM) algorithm using Pearson's correlation coefficient as a distance measure. The initialization and learning parameters of the SOM as well as the neighborhood, topology, and radius were set to the default values suggested by Sturn (2000). However, the dimensions of the SOM network were $2_X * 1_Y$ and were determined by comparing a variety of settings. The SOM algorithm was initiated using randomly selected genes and was allowed to proceed through 123,000 iterations, giving an average of 1000 iterations per gene.

Biological process gene ontologies for the 123 candidate gene list were collected using the Database for Annotation, Visualization and Integrated Discovery (DAVID; apps1.niaid.nih.gov/david). Because genes often fit into more than one ontology category, we present our ontology data in several different ways that address this lack of discreteness. Ultimately, a scheme for ranking the ontologies was developed in order to force each gene into only one category (see Fig. 2d). For example, when possible, more specific categories such as ion transport were given higher priority than more general categories such as transport.

2.5. RT-PCR

cDNA synthesis was performed with the Bio-Rad I-SCRIPT cDNA synthesis kit according to manufacturer instructions. The same total RNA used for microarray hybridizations was used for all subsequent RT-PCR reactions. One of the three RNA samples was chosen from time points 0, 2, and 12 to perform RT-PCR. Oligonucleotide primers for differentially expressed keratin genes were designed using Primer3 (Rozen and Skaletsky, 2000; Table 1; Table 2) such that amplified fragments encompassed their respective GeneChip probe set regions. PCR

Table 1
Primers used for RT-PCR

Contig ID	Gene name	Primer sequence
TC01472_F	Keratin 4	TGT GTC TGT TGG AGG GTG AA
TC01472_R	Keratin 4	ACA GCC ACT GAG CTA CGG TT
MC02467_F	Keratin 6A	CTC AAA AGC CAA CAG GAA GC
MC02467_R	Keratin 6A	CCT GGT AGT CAC GCA GTT GA
TC03778_F	Keratin 6E	TGA TCC CGA AAT CCA GAA AG
TC03778_R	Keratin 6E	CTC ATT CTC TGC AGC TGT GC
MC00232_F	Keratin 6L	CCT CTC TGG TGA ACC AGT CC
MC00232_R	Keratin 6L	CCT GCA CTT TCG GTT GAA AT
MC00098_F	Keratin 12	CAG AAC GTA GAG GCC GAC AT
MC00098_R	Keratin 12	TCC TGA GAG ATC GCT GCT TT
MC00279_F	Keratin 14	TGC AGT CCC AAC TGT CAA TG
MC00279_R	Keratin 14	GAT CCT GAG CCC CCA TCC
MC01260_F	Keratin 15	TCC TCT GTC ACG ATA GTG CG
MC01260_R	Keratin 15	GAA ACA GAA GGT CGC TAC GG
MC00277_F	Keratin 17	AAA CCA TCG ACG ACC TCA AG
MC00277_R	Keratin 17	ATC TCA ACA CTC ACG TCC CC
TC02870_F	Keratin 24	GAA CGA GCA GAA ACT ACG CC
TC02870_R	Keratin 24	CAG CTT CTC GCT CTT TTG CT
MC01187_F	GAPDH	CCA GGC GGC AGG TCA AGT CAA C
MC01187_R	GAPDH	GTC GGC AAG GTC ATC CCA GAG C

Contig IDs represent curated salamander EST assemblies with F indicating the 5′ primer and R indicating the 3′ primer. Gene names represent the common name for the best human RefSeq protein sequence. GAPDH stands for the transcript *glyceraldehyde-3-phosphate dehydrogenase*.

was performed using cDNA generated from 20 ng total RNA and 50 nM forward and reverse primers. PCR parameters for MC01187, MC00098, MC01260, MC00277, TC01472, MC02467, MC00279, and TC02870 were 28 cycles 94 °C for 45 s, 55 °C for 45 s, 72 °C for 30 s, and 72 °C for 5 min. PCR parameters for TC03778 and MC00232 were as above for 26 cycles. 3 μL PCR product was analyzed on 1.2% agarose gels alongside a Genemate 100 base pair ladder and visualized with a Gel Logic 100 Imaging system. PCR product was compared with a control gene (*GAPDH*: MC01187) that showed no significant change across times in the microarray experiment.

3. Results

3.1. Morphological metamorphosis

Although *A. mexicanum* do not normally undergo metamorphosis in the laboratory, metamorphosis can be induced with T4. Salamanders that were sampled after 2 days of T4 treatment showed no external morphological signs of having initiated metamorphosis (Stage 0, Cano-Martinez et al., 1994); thus, they were morphologically identical to day 0 control salamanders. Salamanders that were sampled after 12 days of T4 treatment showed early morphological signs of metamorphosis (reduction of tail fins and gill reduction; Stages I to II). The group of individuals that were sampled after 27 days of T4 treatment had completed metamorphosis, having fully resorbed all external gills and larval tail fins (Stage IV). Thus, 50 nM T4 concentration was sufficient to induce complete metamorphosis in all salamanders.

3.2. Evaluation of the Ambystoma GeneChip

We evaluated the repeatability of the Ambystoma GeneChip by calculating Pearson's *r* for a group of 21 probe sets that were replicated on each chip five times. Correlation matrices were generated for the four triplicate sets of chips that correspond to each sampling time and descriptive statistics were calculated for each matrix ($n=3$, mean r day 0 ± S.E. = 0.953 ± 0.022, $n=3$, mean r day 2 ± S.E. = 0.998 ± 0.001, $n=3$, mean r day 12 ± S.E. = 0.996 ± 0.001, mean r day 28 ± S.E. = 0.990 ± 0.005). These results demonstrate that the repeatability of a given treatment across chips is extremely high.

Table 2
Keratin probe sets evaluated by RT-PCR

Probe ID	Contig ID	Human BLASTX hit	E-value	Human hit GI number
SRV_12057_at *	TC01472	Keratin 4	3.5E−46	gi|17318574|
SRV_02579_a_at *	MC02467	Keratin 6A	7E−120	gi|5031839|
SRV_14426_at	TC03778	Keratin 6E	2.6E−93	gi|27465517|
SRV_00344_at	MC00232	Keratin 6L	3.2E−10	gi|32567786|
SRV_00210_x_at *	MC00098	Keratin 12	1.5E−86	gi|4557699|
SRV_00391_a_at *	MC00279	Keratin 14	6.1E−21	gi|15431310|
SRV_01372_a_at *	MC01260	Keratin 15	7.5E−46	gi|24430190|
SRV_00389_a_at *	MC00277	Keratin 17	1.4E−80	gi|4557701|
SRV_13498_s_at *	TC02870	Keratin 24	2.4E−78	gi|9506669|

* Statistically significant as assessed by ANOVA after controlling for multiple testing using a false discovery rate (FDR) threshold of 0.001.

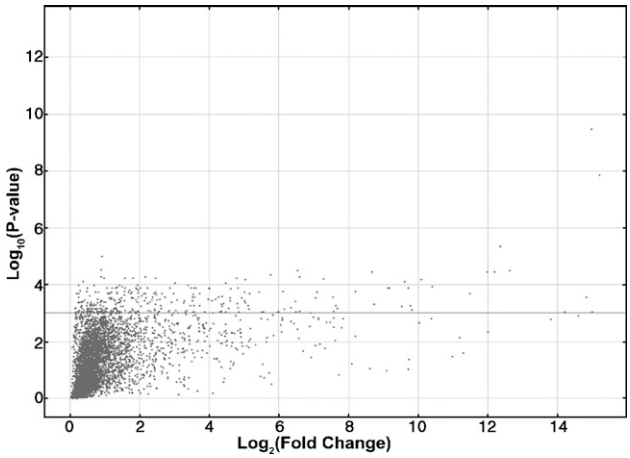

Fig. 1. Volcano plot of the 4844 probe sets on our Affymetrix arrays that were tested for significant differences in hybridization intensity (transcript abundance) across time via ANOVA. Points below the dark horizontal line are not significant after adjusting the FDR to 0.001.

3.3. Identification of TH responsive genes

A total of 325 probe sets yielded significantly different hybridization intensities (transcript abundances) between time points (Fig. 1). To reduce this number and focus attention on probe sets with annotation, we only retained probe sets that were up- or down-regulated by at least 2 fold and which exhibited significant sequence identity (<e−7) with a human reference sequence. Applying these additional criteria reduced the number of significant probe sets (genes) to 123 (Tables 3 and 4). This final list includes a relatively large number of genes (28%) whose protein products are associated uniquely with a single biological process category (Fig. 2a). However, because proteins often have dual or multiple functions, overall we identified 265 functional ontologies and a relatively large number of biological process categories. These results show that TH induced metamorphosis in *A. mexicanum* skin affects the relative abundance of transcripts for loci that presumably function in a variety of molecular, cellular, and developmental contexts (Fig. 2b–d).

3.4. Identification of gene clusters

The SOM analysis identified two clusters of genes that correspond well to up-regulation (Cluster 1; Fig. 3a) and down-regulation (Cluster 2; Fig. 3b). In either cluster, only a few genes exhibited >2 fold changes in transcript abundance, and only one gene exhibited a >3 fold change after 2 days of TH treatment (*solute carrier family 6, member 14*). Thus, we observed no morphological-level changes and very few molecular-level changes at day 2. However by day 12, transcript levels for many genes had changed dramatically. For example, >100–1000 fold changes were measured for *keratin 4*, *keratin 12*, *keratin 14*, and *keratin 24* (Figs. 4 and 5). Two additional

Table 3
List of 62 up-regulated genes showing best BLAST hits and expression levels

Clone ID	Sal ID	BLASTX (E)	Human hit	Gene name	Day 2	Day 12	Day 28
SRV_00391_a_at	MC00279	6.1E−21	gi|15431310|ref|NP_000517.2|	Keratin 14	1.25	1.36×10^3	1.73×10^3
SRV_13498_s_at	TC02870	2.4E−78	gi|9506669|ref|NP_061889.1|	Keratin 24	0.931	901	1.67×10^3
SRV_12057_at	TC01472	3.5E−46	gi|17318574|ref|NP_002263.1|	Keratin 4	1.05	345	418
SRV_03196_a_at	MC03084	3E−69	gi|6005715|ref|NP_009162.1|	Solute carrier family 6, member 14	12.6	68.6	67.4
SRV_00113_at	MC00001	3E−21	gi|66932947|ref|NP_000005.2|	Alpha-2-macroglobulin	1.23	6.23	19.0
SRV_02298_at	MC02186	1.1E−11	gi|40789261|ref|NP_004685.2|	Solute carrier family 16, member 6	1.26	3.39	9.18
SRV_11102_at	TC00532	3.6E−48	gi|4503559|ref|NP_001414.1|	Epithelial membrane protein 1	2.17	17.3	8.82
SRV_11642_at	TC01065	1.5E−21	gi|48255907|ref|NP_001001522.1|	Transgelin	0.978	3.52	8.03
SRV_01767_at	MC01655	2.1E−74	gi|48255907|ref|NP_001001522.1|	Transgelin	0.815	3.75	7.99
SRV_05575_at	MC05458	1.1E−15	gi|21717822|ref|NP_663627.1|	WAP four-disulfide core domain 5	2.22	23.2	7.05
SRV_00504_at	MC00392	4E−161	gi|21361181|ref|NP_000692.2|	ATPase, Na+/K+ transporting	1.38	4.50	6.68
SRV_04813_a_at	MC04696	4.1E−95	gi|21359960|ref|NP_112186.2|	Bubblegum related protein	0.677	3.05	6.27
SRV_00309_at	MC00197	9.9E−15	gi|4507475|ref|NP_000350.1|	Transglutaminase 1	2.63	14.5	6.20
SRV_02941_at	MC02829	1.2E−45	gi|24475847|ref|NP_006460.2|	Influenza virus NS1A binding protein	1.52	1.36	6.11
SRV_02773_at	MC02661	9.8E−31	gi|5174623|ref|NP_006016.1|	26 serine protease	2.02	6.47	5.90
SRV_04996_at	MC04879	1.9E−52	gi|31543641|ref|NP_116192.3|	Solute carrier family 7, member 3	0.451	6.39	4.94
SRV_00466_a_at	MC00354	8.1E−24	gi|4502025|ref|NP_000679.1|	Aminolevulinate, delta-, synthase 1	1.34	4.03	4.81
SRV_10889_at	TC00327	8.9E−54	gi|15147326|ref|NP_000753.2|	Cytochrome P450, family 2	0.841	0.721	4.57
SRV_01521_at	MC01409	1.4E−16	gi|4505865|ref|NP_002650.1|	Plasminogen activator	1.85	5.08	4.55
SRV_00555_at	MC00443	7.2E−44	gi|24307877|ref|NP_000932.1|	P450 (cytochrome) oxidoreductase	0.975	1.77	4.49
SRV_11441_at	TC00864	1.6E−80	gi|13124875|ref|NP_074035.1|	Myosin, heavy polypeptide 11	0.696	1.80	3.90
SRV_02009_at	MC01897	6.5E−61	gi|31982936|ref|NP_003892.2|	Sphingosine-1-phosphate lyase 1	1.24	4.93	3.54
SRV_04923_at	MC04806	5.7E−62	gi|14150098|ref|NP_115699.1|	Hypothetical protein MGC13102	1.60	7.00	3.48
SRV_04787_s_at	MC04670	2.8E−29	gi|4505595|ref|NP_002566.1|	Serine proteinase inhibitor, member 2	1.58	3.76	3.43
SRV_00469_at	MC00357	1.5E−61	gi|25777732|ref|NP_000681.2|	Aldehyde dehydrogenase 2 family	0.977	2.39	3.39
SRV_01215_a_at	MC01103	1.8E−32	gi|4507015|ref|NP_001850.1|	Solute carrier family 31, member 1	1.12	6.06	3.19
SRV_00470_at	MC00358	5.5E−83	gi|25777732|ref|NP_000681.2|	Aldehyde dehydrogenase 2 family	1.21	2.20	3.10
SRV_04693_a_at	MC04576	5E−16	gi|13435361|ref|NP_077739.1|	Desmocollin 1	0.878	3.74	3.06
SRV_12418_at	TC01823	1.9E−33	gi|29568111|ref|NP_006088.2|	Myosin, light polypeptide 9, regulatory	0.815	1.79	2.99
SRV_02418_at	MC02306	1.4E−34	gi|4826902|ref|NP_005015.1|	Serine proteinase inhibitor, member 10	1.79	3.24	2.98
SRV_01550_at	MC01438	8E−100	gi|4506091|ref|NP_002739.1|	Mitogen-activated protein kinase 6	1.70	12.6	2.95
SRV_05319_at	MC05202	7.8E−99	gi|4507953|ref|NP_003397.1|	Tyrosine 3-monooxygenase activator	1.23	2.91	2.79
SRV_01045_a_at	MC00933	6.9E−54	gi|4501883|ref|NP_001604.1|	Actin, alpha 2, smooth muscle, aorta	0.579	1.41	2.71
SRV_00439_at	MC00327	6.4E−77	gi|23065544|ref|NP_000552.2|	Glutathione *S*-transferase M1	1.00	2.85	2.69
SRV_01121_at	MC01009	7.8E−91	gi|24638454|ref|NP_733765.1|	ATPase, Ca2+ transporting	1.06	4.07	2.67
SRV_02178_a_at	MC02066	7.5E−34	gi|4758116|ref|NP_004384.1|	Dystroglycan 1	0.949	4.69	2.66
SRV_05448_at	MC05331	3E−100	gi|24638454|ref|NP_733765.1|	ATPase, Ca2+ transporting	1.20	3.99	2.66
SRV_04119_at	MC04006	1.5E−24	gi|8923678|ref|NP_060427.1|	Epsin 3	0.927	4.61	2.65
SRV_04229_at	MC04116	6.5E−53	gi|8922901|ref|NP_060810.1|	Hypothetical protein FLJ11151	0.966	1.17	2.63
SRV_11152_at	TC00582	1E−124	gi|4501883|ref|NP_001604.1|	Actin, alpha 2, smooth muscle, aorta	0.669	1.52	2.55
SRV_04911_at	MC04794	3.6E−18	gi|42516570|ref|NP_115619.4|	Thioredoxin domain containing 2	1.13	2.44	2.54
SRV_14223_at	TC03582	9.8E−72	gi|21264315|ref|NP_644670.1|	EH-domain containing 4	1.16	9.87	2.48
SRV_03255_a_at	MC03143	0.000000019	gi|6912280|ref|NP_036243.1|	Act. of hsp 90 kDa ATPase	1.43	3.42	2.42
SRV_03491_a_at	MC03379	8E−68	gi|7657118|ref|NP_055106.1|	Glycine C-acetyltransferase	0.766	1.11	2.31
SRV_03562_at	MC03450	7.3E−33	gi|7657069|ref|NP_055399.1|	ERO1-like	1.16	4.23	2.27
SRV_02177_at	MC02065	4E−75	gi|4758116|ref|NP_004384.1|	Dystroglycan 1	1.21	3.43	2.20
SRV_03398_at	MC03286	2E−133	gi|45545411|ref|NP_995314.1|	NCK-associated protein 1	1.01	1.21	2.18
SRV_04215_at	MC04102	5.2E−44	gi|63055049|ref|NP_060760.2|	Phosphoglucomutase 2	0.904	1.02	2.11
SRV_02554_at	MC02442	1.1E−50	gi|4885495|ref|NP_005485.1|	DnaJ (Hsp40) homolog, member 6	1.00	2.50	2.07
SRV_11893_a_at	TC01316	6E−21	gi|4757962|ref|NP_004055.1|	Cyclin-dependent kinase inhibitor 1B	1.33	2.95	2.01
SRV_02461_at	MC02349	3.2E−34	gi|24307889|ref|NP_005144.1|	Ubiquitin specific protease 10	1.18	2.04	2.01
SRV_08154_a_at	MC08037	8.5E−12	gi|24234688|ref|NP_004125.3|	Heat shock 70 kDa protein 9B	1.10	2.88	1.99
SRV_02108_a_at	MC01996	8E−68	gi|47419916|ref|NP_776049.1|	Tryptophanyl-tRNA synthetase	1.10	2.80	1.89
SRV_02310_at	MC02198	1E−101	gi|4759034|ref|NP_004721.1|	Euk. translation termination factor 1	1.24	3.24	1.88
SRV_02093_a_at	MC01981	1.7E−65	gi|24234688|ref|NP_004125.3|	Heat shock 70 kDa protein 9B	1.22	2.61	1.84
SRV_02201_at	MC02089	8.2E−70	gi|4758340|ref|NP_004452.1|	Phenylalanine-tRNA synthetase-like	1.05	2.40	1.83
SRV_05178_at	MC05061	6.2E−44	gi|18254466|ref|NP_543143.1|	Suppressor of cytokine signaling 4	1.16	3.08	1.76
SRV_05297_at	MC05180	6.7E−93	gi|21618349|ref|NP_659731.1|	MAP kinase kinase 3	1.25	5.11	1.73
SRV_02203_a_at	MC02091	2.4E−59	gi|17149844|ref|NP_476433.1|	FK506 binding protein 2, 13 kDa	1.22	2.19	1.68
SRV_02289_a_at	MC02177	2.6E−20	gi|4758984|ref|NP_004654.1|	RAB11A, member RAS family	1.33	3.53	1.51
SRV_04798_a_at	MC04681	4.5E−22	gi|23308607|ref|NP_110416.1|	Histocompatibility (minor) 13	0.841	2.32	1.33
SRV_12195_at	TC01606	5.8E−58	gi|56119207|ref|NP_005223.3|	EphA1	1.19	2.00	1.11

Sal IDs correspond to *Ambystoma mexicanum* contigs used for probe production. Sequence similarity was assessed using the entire contig sequence. Day 2, day 12, and day 28 columns are the average fold changes compared to day 0.

Table 4
List of 61 down-regulated genes showing best BLAST hits and expression levels

Clone ID	Sal ID	BLASTX (E)	Human hit	Gene name	Day 2	Day 12	Day 28
SRV_02216_a_at	MC02104	2.5E−11	gi|9845516|ref|NP_062427.1|	S100 calcium binding protein A4	−0.981	-1.52×10^{2}	-3.40×10^{2}
SRV_00210_x_at	MC00098	1.5E−86	gi|4557699|ref|NP_000214.1|	Keratin 12	−1.14	−67.4	−131
SRV_00221_x_at	MC00109	1.7E−59	gi|4557699|ref|NP_000214.1|	Keratin 12	−1.15	−68.7	−111
SRV_10623_x_at	TC00107	4.7E−86	gi|4557699|ref|NP_000214.1|	Keratin 12	−1.12	−69.1	−106
SRV_02579_a_at	MC02467	7E−120	gi|5031839|ref|NP_005545.1|	Keratin 6A	−1.38	−111	−99.1
SRV_00205_a_at	MC00093	1.4E−56	gi|4557699|ref|NP_000214.1|	Keratin 12	−1.10	−40.8	−95.2
SRV_02006_a_at	MC01894	3E−49	gi|4503681|ref|NP_003881.1|	Fc fragment of IgG binding protein	1.11	−94.2	−87.0
SRV_03122_a_at	MC03010	3.5E−68	gi|49619237|ref|NP_008883.2|	Uroplakin 1B	1.06	−28.7	−55.2
SRV_03130_a_at	MC03018	2.8E−79	gi|5902148|ref|NP_008931.1|	Uroplakin 1A	−1.11	−13.1	−40.7
SRV_02688_at	MC02576	8.1E−21	gi|53988380|ref|NP_037536.2|	Mesothelin	−1.35	−30.1	−39.7
SRV_03123_at	MC03011	3.9E−37	gi|49619237|ref|NP_008883.2|	Uroplakin 1B	1.18	−21.7	−33.2
SRV_05278_a_at	MC05161	1.1E−40	gi|24638435|ref|NP_653273.2|	Otoancorin	−1.79	−15.5	−29.4
SRV_01482_at	MC01370	2.3E−41	gi|4505621|ref|NP_002558.1|	Prostatic binding protein	−1.71	−6.03	−20.6
SRV_05485_a_at	MC05368	1.3E−14	gi|38490577|ref|NP_941963.1|	Keratin associated protein 18–9	−1.07	−22.3	−20.2
SRV_00389_a_at	MC00277	1.4E−80	gi|4557701|ref|NP_000413.1|	Keratin 17	1.37	−1.56	−16.0
SRV_12633_a_at	TC02028	8.4E−81	gi|58218968|ref|NP_005175.2|	Calmodulin 1	−1.37	−11.8	−12.3
SRV_01372_a_at	MC01260	7.5E−46	gi|24430190|ref|NP_002266.2|	Keratin 15	−1.14	−6.81	−11.0
SRV_01410_a_at	MC01298	6.7E−48	gi|4505091|ref|NP_002362.1|	mal, T-cell differentiation protein	−1.16	−5.07	−11.0
SRV_13669_at	TC03037	6E−64	gi|10864037|ref|NP_067046.1|	Myosin, light polypeptide 7, regulatory	−1.07	−3.19	−10.5
SRV_01220_at	MC01108	1E−31	gi|4502985|ref|NP_001854.1|	Cytochrome *c* oxidase subunit VIb	1.08	1.29	−7.65
SRV_02072_at	MC01960	6.4E−50	gi|23110962|ref|NP_004070.3|	Cathepsin S	−1.08	−1.48	−6.73
SRV_00038_at	gi|4325096	4E−27	NP_000890.1	KIT ligand	−1.42	−9.89	−6.52
SRV_05180_a_at	MC05063	7.9E−41	gi|46409392|ref|NP_997267.1|	QRWT5810	−2.01	−7.21	−5.84
SRV_02056_a_at	MC01944	6.6E−18	gi|4757826|ref|NP_004039.1|	Beta-2-microglobulin	−1.08	−2.67	−5.55
SRV_01687_at	MC01575	9.4E−24	gi|22538814|ref|NP_002976.2|	Chemokine (C-C motif) ligand 5	1.20	−5.48	−5.28
SRV_02292_at	MC02180	0.000000092	gi|4758814|ref|NP_004679.1|	N-myc (and STAT) interactor	−1.02	−3.23	−4.88
SRV_03421_a_at	MC03309	2E−11	gi|21361501|ref|NP_054739.2|	LR8 protein	−1.19	−4.29	−4.70
SRV_00387_at	MC00275	8.2E−61	gi|4504373|ref|NP_000512.1|	Hexosaminidase B	−1.19	−2.76	−4.60
SRV_14350_at	TC03706	2.2E−70	gi|23510391|ref|NP_002489.1|	NIMA-related kinase 3	−1.16	−4.71	−3.55
SRV_01294_at	MC01182	3.3E−71	gi|56682959|ref|NP_002023.2|	Ferritin, heavy polypeptide 1	1.00	−1.34	−3.46
SRV_04183_at	MC04070	1.5E−43	gi|46397369|ref|NP_997002.1|	Leucine rich repeat containing 20	−1.02	−2.36	−3.25
SRV_00512_at	MC00400	5.6E−32	gi|13787189|ref|NP_000761.2|	Cytochrome P450	−1.24	−1.15	−3.15
SRV_03763_at	MC03651	1.5E−84	gi|56606000|ref|NP_001008398.1|	Similar to 2310016C16Rik protein	−1.17	−4.22	−3.01
SRV_05463_at	MC05346	3.4E−94	gi|26051208|ref|NP_742076.1|	CaM kinase II beta	1.05	−3.15	−2.94
SRV_00527_at	MC00415	2.7E−62	gi|23065557|ref|NP_671489.1|	Glutathione *S*-transferase M4	−1.32	−3.63	−2.93
SRV_01306_at	MC01194	2.5E−29	gi|4504025|ref|NP_002055.1|	Glutaredoxin (thioltransferase)	1.09	−1.51	−2.87
SRV_00135_at	MC00023	2.2E−23	gi|4557335|ref|NP_000040.1|	Aspartoacylase	−1.22	−3.63	−2.77
SRV_05460_at	MC05343	7E−65	gi|25777698|ref|NP_742013.1|	Tripartite motif-containing 39	−1.10	−2.62	−2.73
SRV_02285_at	MC02173	2.7E−55	gi|5031691|ref|NP_004640.1|	Chromosome 21 o.r.f. 33	−1.10	−1.21	−2.62
SRV_03073_at	MC02961	2.4E−36	gi|21361310|ref|NP_006408.2|	Interferon-induced protein 44	−1.13	−2.25	−2.27
SRV_01633_at	MC01521	4.3E−90	gi|4506381|ref|NP_002863.1|	ras-related botulinum toxin substrate 2	−1.13	−1.17	−2.26
SRV_00098_at	–	5E−11	CAA52857	Ax_xVent_5.1	−1.11	−2.16	−2.16
SRV_05077_at	MC04960	2.7E−31	gi|55769559|ref|NP_008893.1|	Zinc finger protein 21 (KOX 14)	1.02	−2.72	−2.09
SRV_05450_a_at	MC05333	1.2E−38	gi|24762248|ref|NP_733778.1|	Integrin beta 1 binding protein 3	−1.01	−1.77	−2.04
SRV_00148_at	MC00036	3E−16	gi|4503107|ref|NP_000090.1|	Cystatin SA	−1.04	−2.12	−1.92
SRV_03769_a_at	MC03657	9.5E−20	gi|7705662|ref|NP_056955.1|	Zinc finger protein 593	−1.04	−3.27	−1.80
SRV_05597_at	MC05480	8E−41	gi|32698876|ref|NP_872329.1|	Hypothetical protein MGC61571	−1.01	−2.30	−1.76
SRV_03144_at	MC03032	1.2E−63	gi|5902034|ref|NP_008993.1|	Nuclear phosphoprotein PWP1	1.15	−2.94	−1.73
SRV_05231_at	MC05114	1.4E−22	gi|42476216|ref|NP_620142.2|	Hypothetical protein BC009561	1.00	−2.29	−1.70
SRV_04972_a_at	MC04855	6.5E−45	gi|14211923|ref|NP_115982.1|	Histidine triad nucleotide bind. protein 2	−1.16	−3.35	−1.65
SRV_03843_a_at	MC03731	9.7E−57	gi|7705592|ref|NP_057144.1|	CGI-125 protein	−1.11	−2.15	−1.52
SRV_05174_a_at	MC05057	1.6E−36	gi|63079718|ref|NP_542432.2|	Three prime repair exonuclease 2	2.13	−0.145	−1.49
SRV_05237_at	MC05120	1.1E−76	gi|20270341|ref|NP_620149.1|	Lysophospholipase-like 1	1.02	−2.47	−1.49
SRV_05090_at	MC04973	3.8E−53	gi|29789285|ref|NP_444269.1|	COMM domain containing 7	1.04	−2.53	−1.43
SRV_01556_at	MC01444	8E−126	gi|4506129|ref|NP_002756.1|	Phosphoribosyl pyrophosphate synth. 2	−1.17	−2.24	−1.35
SRV_04181_at	MC04068	3E−112	gi|8922633|ref|NP_060670.1|	High-mobility group 20A	−1.17	−2.43	−1.29
SRV_05010_at	MC04893	2.9E−43	gi|14249632|ref|NP_116270.1|	U7 small nuclear RNA associated	−1.07	−2.73	−1.29
SRV_03429_a_at	MC03317	5.5E−23	gi|7662639|ref|NP_054770.1|	Transmembrane protein 14A	−1.20	−2.26	−1.25
SRV_03369_at	MC03257	1.5E−71	gi|7019465|ref|NP_037462.1|	Expressed in non-metastatic cells 7	1.08	−2.05	−1.21
SRV_01958_at	MC01846	7.4E−35	gi|4503537|ref|NP_003723.1|	Euk. translation initiation factor 4E bp 3	1.08	−2.07	−1.11
SRV_00529_a_at	MC00417	3.4E−36	gi|4504183|ref|NP_000843.1|	Glutathione *S*-transferase pi	−1.10	−2.58	1.18

Sal IDs correspond to *Ambystoma mexicanum* contigs used for probe production. Sequence similarity was assessed using the entire contig sequence. Day 2, day 12, and day 28 columns are the average fold changes compared to day 0.

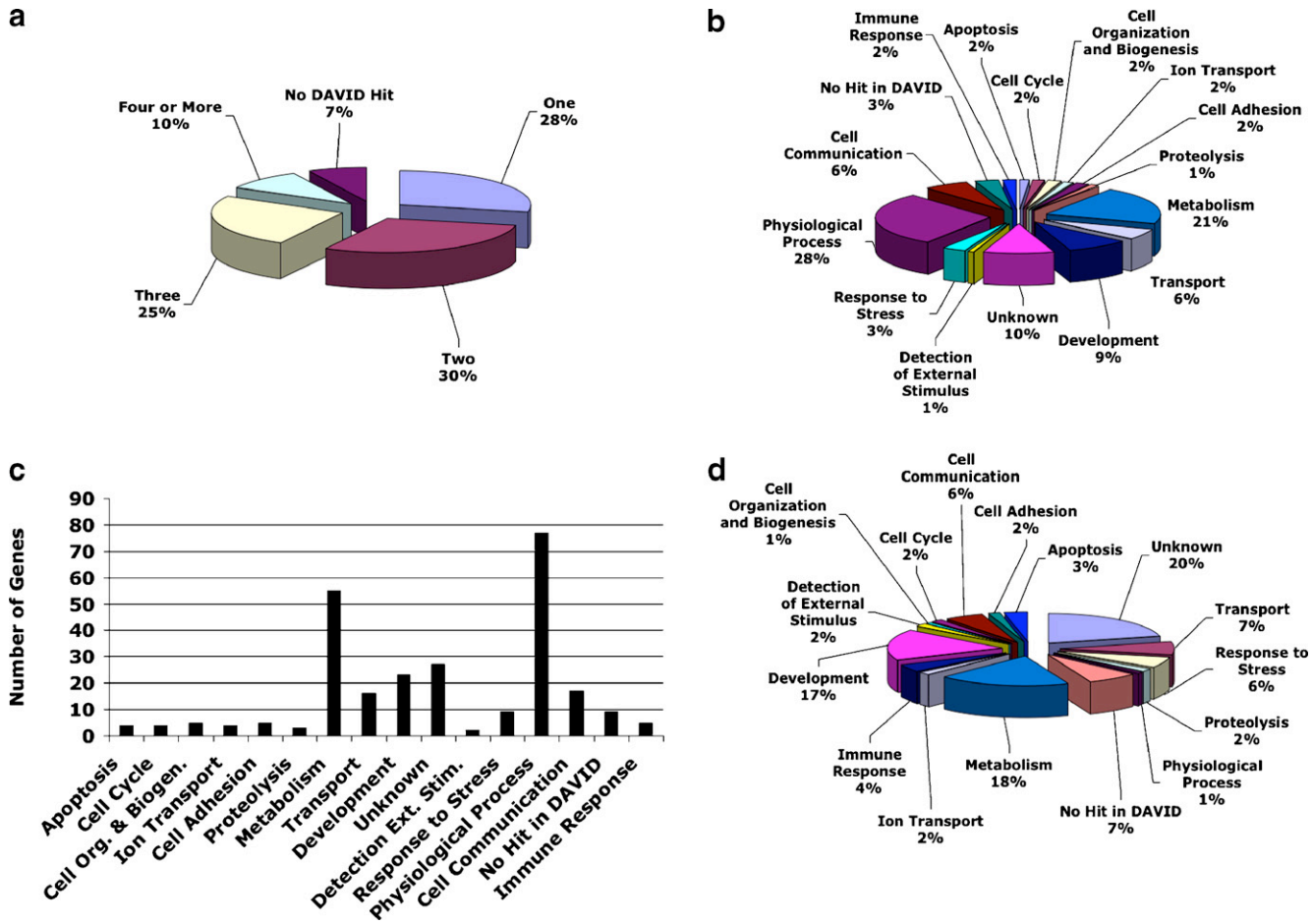

Fig. 2. Graphical representation of the gene ontologies for 123 probe sets. (a) The proportion of genes that fit into one, two, three, or four or more biological process categories. (b) The proportion of the 265 ontologies that fit into each category. The mean number of ontologies per gene = 2.15. (c) The number of genes that are located in each of the ontology categories. Some genes are in more than one category. (d) The proportion of genes that are in each category when genes are assigned to only one category. Assignments were made in decreasing order of priority from the following list (i.e., one is highest priority): (1) apoptosis, (2) development, (3) immune response, (4) detection of external stimulus, (5) response to stress, (6) cell adhesion, (7) cell organization and biogenesis, (8) cell communication, (9) cell cycle, (10) ion transport, (11) transport, (12) proteolysis, (13) metabolism, (14), physiological process, (15) unknown, (16) no hit in DAVID.

keratins and a keratin-associated protein were also identified as significantly regulated. Our results show that the relative abundances of transcripts for several members of the keratin gene family change dramatically in TH induced *A. mexicanum* at the time of morphological remodeling of the epidermis.

3.5. RT-PCR of keratins

RT-PCR was used as an independent method of gene expression analysis to evaluate significant microarray results for the first 3 time periods (days 0, 2, 12). We focused our efforts on the differentially expressed keratins because independent confirmation by RT-PCR would further support the idea that these keratins are sensitive biomarkers of TH induction (Figs. 4 and 5). GAPDH was used as a reference gene because it was not TH responsive in the microarray analysis; this result was confirmed by RT-PCR (Fig. 6). The ~1000 fold increase in transcript abundance that was detected by microarray analysis for *keratin 4, keratin 14,* and *keratin 24* on day 12 was convincingly confirmed by RT-PCR as there was no observable PCR product on gels. RT-PCR also confirmed the >10 fold decrease in transcript abundance that was measured for *keratin 6A* and *keratin 12* on day 12. Although average fold-level changes of the remaining keratins were small as measured by microarray analysis (<7), changes in the predicted direction were observed in all cases by RT-PCR. These results confirm that keratin loci are TH responsive and show that major and minor gene expression changes that are measured by the Ambystoma GeneChip are replicable using an independent assay.

4. Discussion

Although there have been several microarray analyses of anuran amphibians, ours is the first using a salamander. The custom GeneChip we developed identified a collection of TH-regulated genes that will enable future studies of post-embryonic development, specifically in the areas of developmental genetics and endocrine disruption. Below, we discuss our results within the context of TH-regulated gene expression

as it applies to amphibian epidermal development and metamorphosis using the Ambystoma model organism system.

4.1. Amphibian skin and TH-induced changes at metamorphosis

The integument or skin of an organism is a very important tissue because it provides the interface between the body and the external environment. Amphibian skin protects the body from many different physical and mechanical stresses, pathogens, and toxic agents, and also performs many vital functions, including structural support, osmoregulation, respiration, mechanoreception, camouflage, and protection from desiccation (Duellman and Trueb, 1986). The epidermis of larval amphibians has the same general structure: an outer layer of apical cells and an inner basal layer (reviewed by Fox, 1983). In

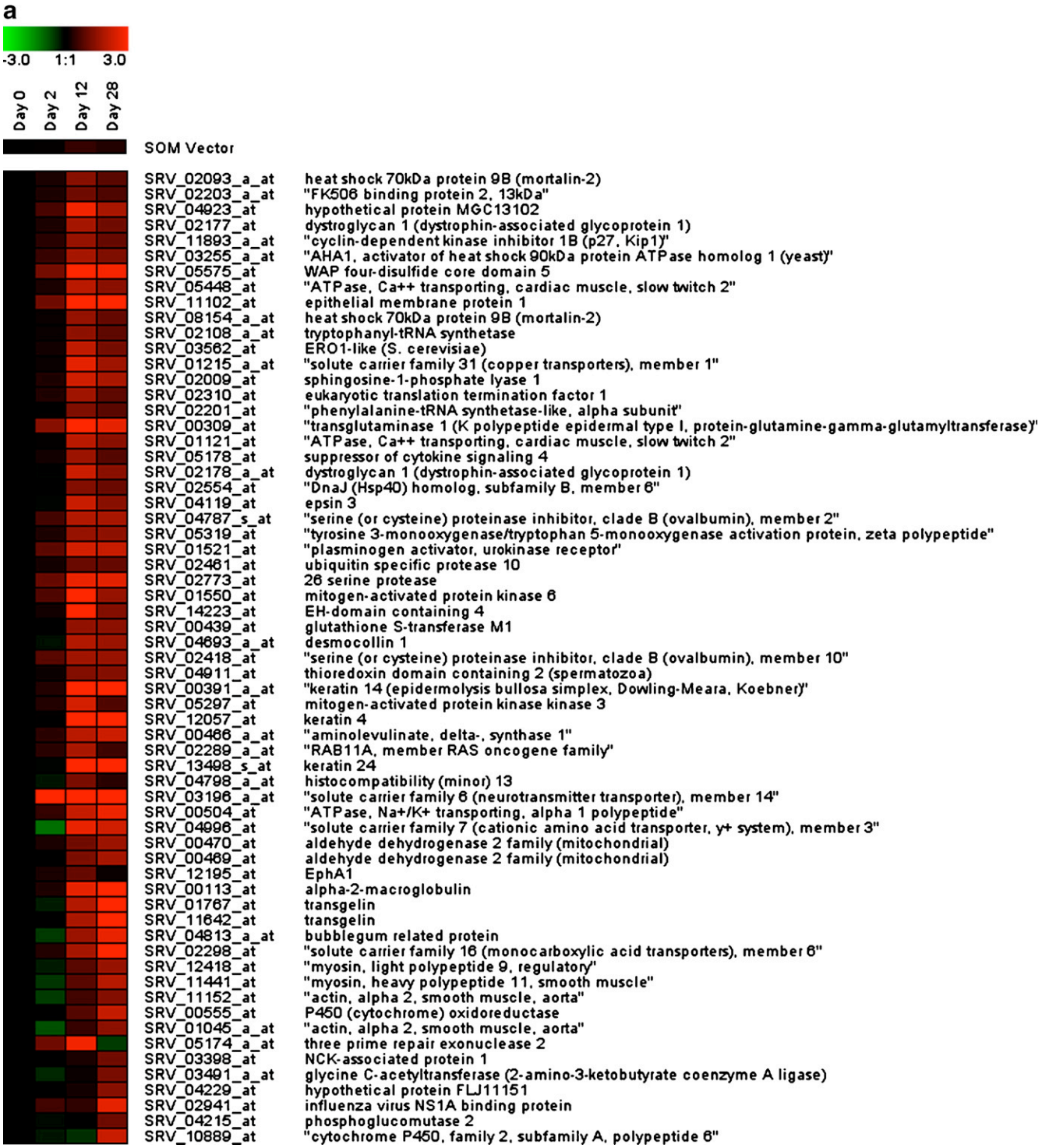

Fig. 3. Expression profiles of the two clusters obtained from the SOM algorithm. (a) Cluster 1 (up regulated) contains 61 genes. (b) Cluster 2 (down regulated) contains 62 genes. Gene names are given based on the best BLASTX hit to the human genome.

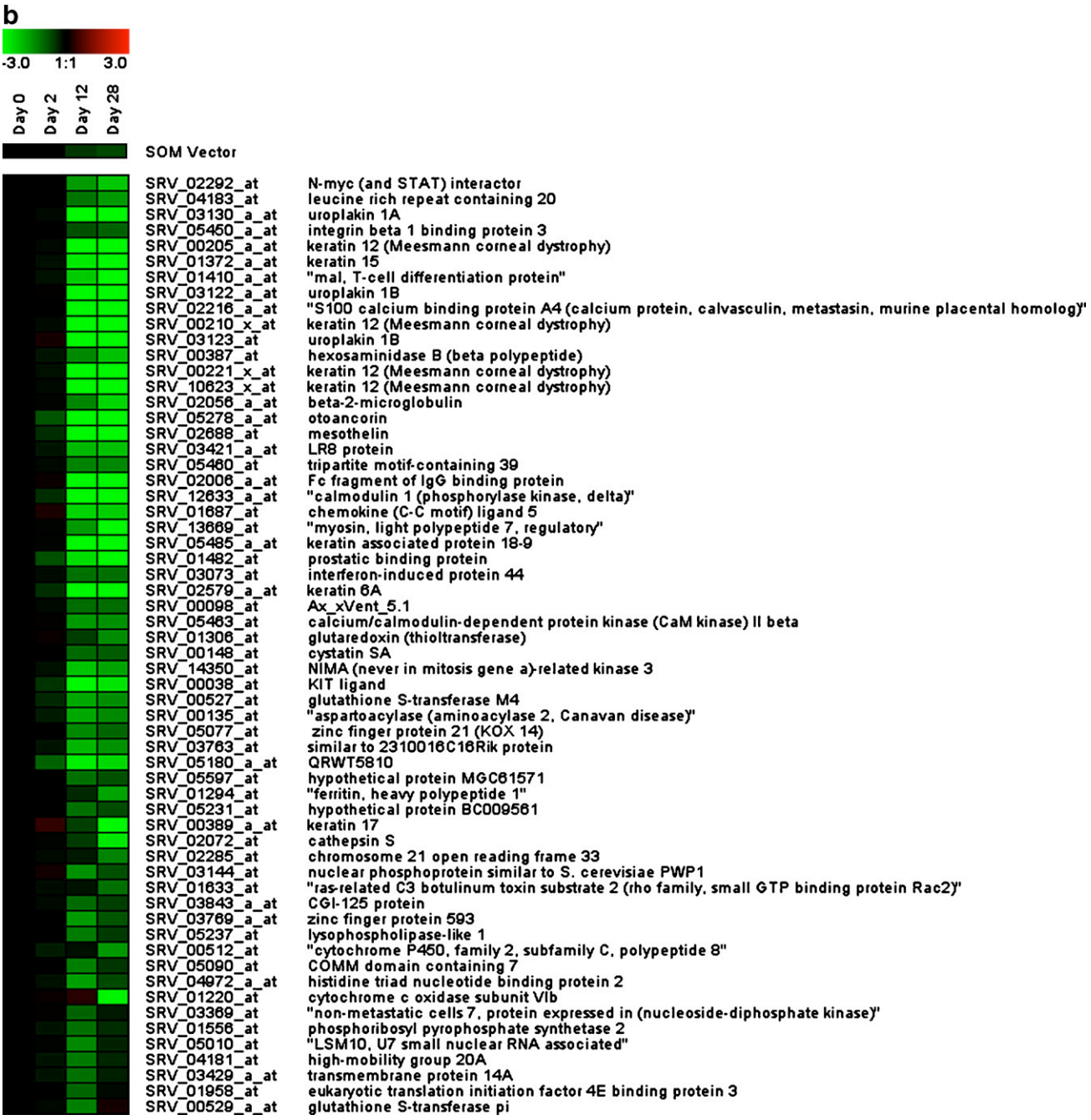

Fig. 3 (*continued*).

salamanders, there is a distinct middle layer of Leydig cells (Kelly, 1966). The basal population includes progenitor cells that ultimately give rise to adult cell types at metamorphosis. There are variations on this general structural theme and considerable variation in the numbers and types of cells among amphibian species.

The larval, metamorphosing, and adult *A. mexicanum* epidermis has been described in detail (Fahrmann (1971a,b,c). The larval epidermis of *A. mexicanum* consists of an apical layer of cover cells, an interstitial layer of mucous secreting Leydig cells, and a basal layer of germinative cells. Other cells of lower relative abundance are distributed in the epidermis, including goblet cells, flask cells, mesenchymal macrophages, fibroblasts, melanocytes, and supporting cells of lateral line neuromasts. During TH-induced metamorphosis, Leydig cells disappear in *A. mexicanum* and *Hynobius retardatus*; the disappearance of Leydig cells in *H. retardatus* is consistent with TH-induced apoptosis (Ohumura and Wakahara, 1998). It is known from extensive studies of larval anurans that TH induces apoptosis and other metamorphic programs by regulating cell-specific patterns of gene expression; TH binds directly to nuclear receptors (and accessory factors) that activate or repress

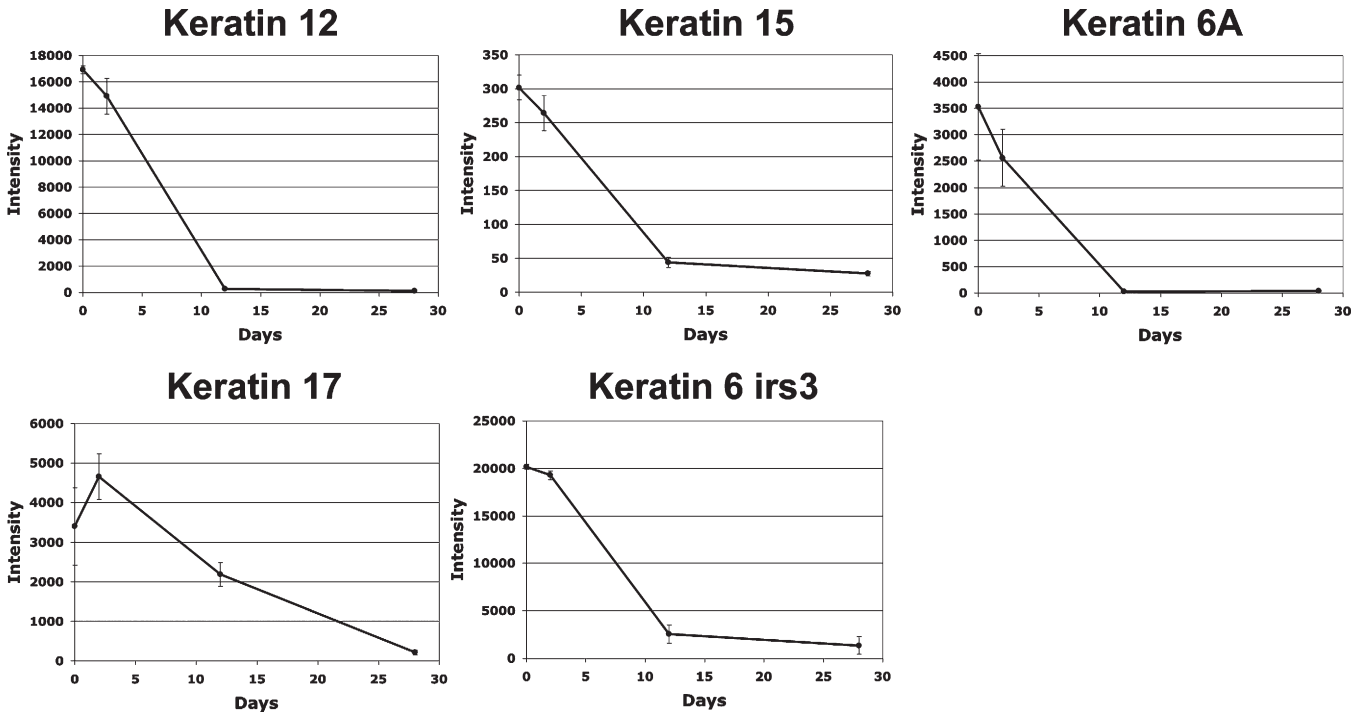

Fig. 4. Down-regulated keratins. The *y*-axis represents intensity (arbitrary units), and the *x*-axis represents days (0, 2, 12, 28). Gene names are given based on the best BLASTX hit to the human genome. Dark circles represent the mean of three samples±S.E.

gene transcription (Shi, 2000; Buchholz et al., 2006). With respect to larval anuran epidermis, TH induces autonomously, apoptotic gene expression programs in outer apical cells (Schreiber and Brown, 2002). This cell population is replaced by a cornified layer of squamous cells that originate from progenitors of the basal cell population (Kinoshita and Sasaki, 1994; Suzuki et al., 2002; Ishida et al., 2003). In addition, TH induces gene expression programs in the basal cell population

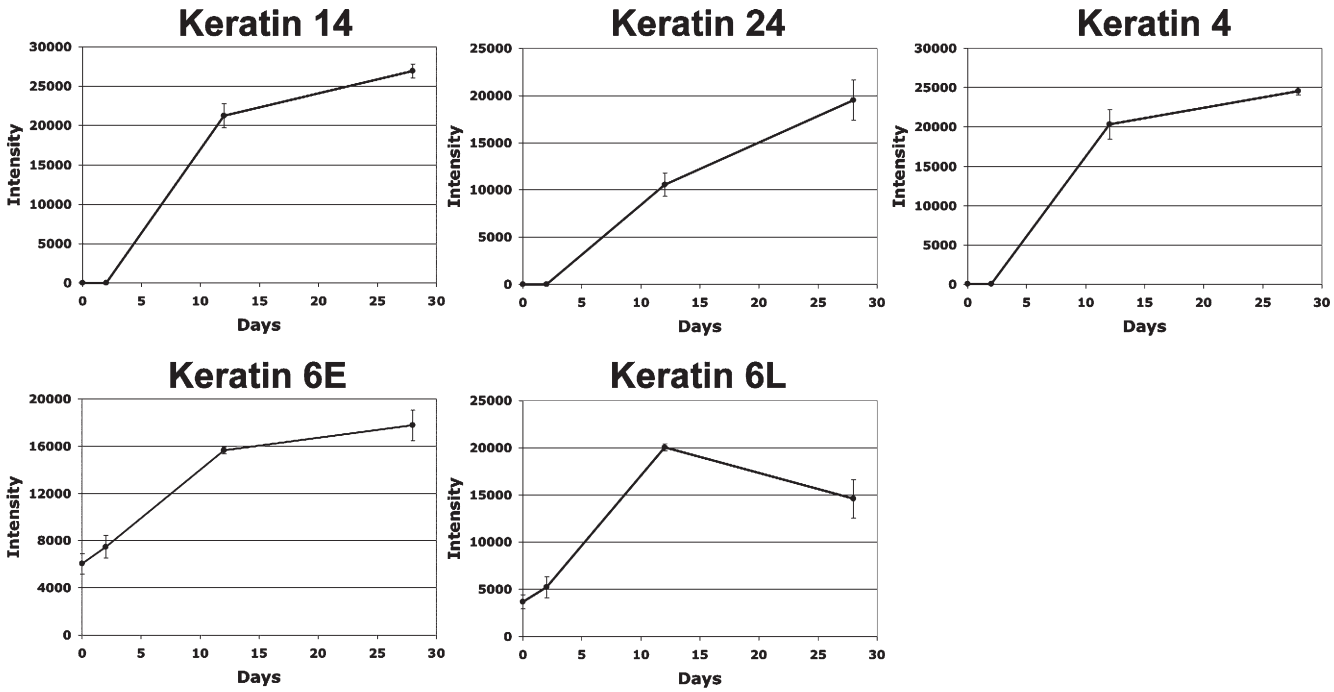

Fig. 5. Up-regulated keratins. The *y*-axis represents intensity (arbitrary units) and the *x*-axis represents days (0, 2, 12, 28). Gene names are given based on the best BLASTX hit to the human genome. Dark circles represent the mean of three samples±S.E.

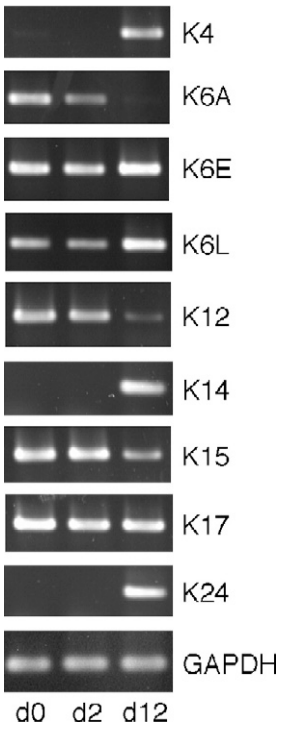

Fig. 6. RT-PCR of keratins. Columns represent 0, 2, and 12 days of T4 treatment.

that reorganizes the collagen lamella and initiate de novo development of skin glands to yield an adult epidermis that is better suited for terrestrial existence.

4.2. TH-induced gene expression in ambystomatid skin

Although our analysis allowed for temporal clustering of genes, the clusters identified differed in transcript abundance: up-regulated versus down-regulated gene clusters. There are at least two reasons why we obtained this clustering result. First, the number of possible clustering outcomes may have been reduced in our experiment because relatively few transcripts were activated or repressed after 2 days of TH treatment. Additional clusters of genes may have been identified if more sampling times were included in the experimental design, especially for periods flanking day 12. Second, it is well known from anuran studies that TH does in fact induce up- and down-regulation of genes in epithelial tissues (Shi, 2000); in other words, the clustering result was obtained because of the known, molecular-level effect of TH. We observed many significant up- and down-regulated gene expression changes by day 12 in *A. mexicanum*, and these coincided with early reductions of fin and gill epithelia. This correlation between morphology and transcript abundance suggests two possible explanations for the classification of genes as down-regulated: (1) These genes (e.g. *keratins 6A*, *12*, *15*) maybe expressed uniquely in Leydig and apical cells that ultimately disappear during metamorphosis. As Leydig and apical cell numbers decrease during metamorphosis, so might the relative abundance of transcripts for larval-specific genes. (2) TH may repress transcription of genes classified as down-regulated in basal cells that survive or differentiate during metamorphosis. With respect to genes classified as up-regulated (e.g. *keratins 4*, *6E*, *6L*, *14*, and *24*), transcript numbers may increase because of transcriptional activation by TH. Although relatively little is known about the molecular functions of keratins during metamorphosis, they are useful biomarkers for epithelial cell differentiation. In this regard, it is well established that TH initiates the switch from larval-type to-adult-type keratin transcription during anuran metamorphosis, and this occurs at the time of basal cell differentiation and cornification of the epidermis (Reeves, 1975; Mathisen and Miller, 1987; Shimizu-Nishikawa and Miller, 1992; Watanabe et al., 2001). Future studies that localize mRNAs to specific cell types by *in situ* hybridization are needed to better understand the temporal regulation of keratin loci during metamorphosis, and gain insight about their molecular functions.

5. Role of skin and microarray analysis in endocrine disruption

Although several biochemical and molecular assays have been proposed as tests for endocrine disruption of the TH axis, morphological endpoint methods are more commonly used in amphibians (e.g. Degitz et al., 2005; Opitz et al., 2005). These methods use pre-prometamorphic and prometamorphic *Xenopus laevis* tadpoles and developmental staging series to evaluate TH induced changes in morphology and developmental timing variation. Our study shows that similar morphological tests can easily be developed for *A. mexicanum* and coupled with gene expression assays. The fold level changes that we measured for several keratin loci during early stages of TH induced metamorphosis in *A. mexicanum* are orders of magnitude greater than thyroid hormone receptor gene expression changes that are observed in comparable anuran-based assays (e.g. Zhang et al., 2006). This suggests that keratin loci are extremely sensitive biomarkers that can be developed to test *A. mexicanum* skin for temporal disruptions of the larval-to-adult gene expression program. They should also be useful for identifying basal progenitor and adult stem cell populations.

6. Ambystoma as a model for endocrine disruption

Our study sets the stage for future gene expression experiments that promise to yield exacting assays for monitoring endocrine disruption in the laboratory and in nature. This later goal is achievable because genome and bioinformatics resources can be extended from the laboratory model *A. mexicanum* to ambystomatids that are widely distributed among diverse aquatic habitats in North America (Putta et al., 2004; Smith et al., 2005). For over 35 years, the National Science Foundation has provided funding to maintain a collection of genetically homogenous *A. mexicanum* for distribution (embryos, larvae, adults, and mutants) to researchers throughout the world. This resource is known as the Ambystoma Genetic Stock Center and it is located at the University of Kentucky (http://bigapple.uky.edu/~axolotl). In contrast to the anuran model Xenopus (African clawed frog), much is known about

the ecology, evolution, and natural history of ambystomatid salamanders and they are indigenous to a diversity of North American habitats. Ambystomatid salamanders are found in the coastal lowlands of the Carolinas, the prairie and central plains of the Midwest, elevations exceeding 10,000 ft in the Rocky Mountains, arid desert-lands of the southwest US and Mexico, and ephemeral natural ponds in California, just to name a few. The diversity of habitats that ambystomatid salamanders occupy makes them an ideal model for studying environmental variables and endocrine disruptors in the field and laboratory.

Acknowledgements

We acknowledge the service of Donna Walls in the UK Microarray Facility. This project was made possible by grant numbers 5R24RR016344, 2P20RR016741, and 2P20RR016481-04 from the National Center for Research Resources, a component of the National Institutes of Health. Its contents are solely the responsibility of the authors and do not necessarily represent the official views of NCRR or NIH. Aspects of this project were also made possible by funding from the U.S. National Science Foundation (IOB-0242833; DBI-0443496) and the Kentucky Spinal Cord and Head Injury Research Trust.

References

Amiel-Tison, C., Cabrol, D., Denver, R., Jarreau, P.H., Papiernik, E., Piazza, P.V., 2004. Fetal adaptation to stress: Part II. Evolutionary aspects; stress-induced hippocampal damage; long-term effects on behavior; consequences on adult health. Early Hum. Dev. 78, 81–94.

Baldessari, D., Shin, Y., Krebs, O., Koenig, R., Koide, T., Vinayagam, A., Fenger, U., Mochii, M., Terasaka, C., Kitayama, A., Peiffer, D., Ueno, N., Eils, R., Cho, K.W., Niehrs, C., 2005. Global gene expression profiling and cluster analysis in *Xenopus laevis*. Mech. Dev. 122, 441–475.

Barrington, E.J.W., 1962. Hormones and vertebrate evolution. Experientia 18, 201–210.

Benjamini, Y., Hochberg, Y., 1995. Controlling the false discovery rate: a practical and powerful approach to multiple testing. J. R. Stat. Soc., Ser. B Stat. Methodol. 57, 289–300.

Brent, G.A., 1994. The molecular basis of thyroid hormone action. N. Engl. J. Med. 331, 847–853.

Buchholz, D.R., Paul, B.D., Fu, L., Shi, Y.B., 2006. Molecular and developmental analyses of thyroid hormone receptor function in *Xenopus laevis*, the African clawed frog. Gen. Comp. Endocrinol. 145, 1–19.

Cano-Martinez, A., Vargas-González, A., Asai, M., 1994. Metamorphic stages in *Ambystoma mexicanum*. Axolotl Newsl. 23, 64–71.

Chalmers, A.D., Goldstone, K., Smith, J.C., Gilchrist, M., Amaya, E., Papalopulu, N., 2005. *Xenopus tropicalis* oligonucleotide microarray works across species using RNA from *Xenopus laevis*. Mech. Dev. 122, 355–363.

Crespi, E.J., Denver, R.J., 2004. Ancient origins of human developmental plasticity. Am. J. Hum. Biol. 17, 44–54.

Crump, D., Werry, K., Veldhoen, N., van Aggelen, G., Helbing, C.C., 2002. Exposure to the herbicide acetochlor alters thyroid hormone-dependent gene expression and metamorphosis in *Xenopus laevis*. Environ. Health Perspect. 110, 1199–1205.

Cui, X., Churchill, G.A., 2003. Statistical tests for differential expression in cDNA microarray experiments. Genome Biol. 4, 210.

Degitz, S.J., Holcombe, G.W., Flynn, K.M., Kosian, P.A., Korte, J.J., Tietge, J.E., 2005. Progress towards development of an amphibian-based thyroid screening assay using *Xenopus laevis*. Organismal and thyroidal responses to the model compounds 6-propylthiouracil, methimazole, and thyroxine. Toxicol. Sci. 87, 353–364.

Denver, R.J., Glennemeier, K.A., Boorse, G.C., 2002. Endocrinology of complex life cycles: amphibians. In: Pfaff, D., Arnold, A., Etgen, A., Fahrbach, S., Moss, R., Rubin, R. (Eds.), Hormones, Brain and Behavior, vol. 2. Academic Press, Inc., San Diego, pp. 469–513.

Duellman, W.E., Trueb, L., 1986. Biology of Amphibians. McGraw Hill, New York.

Fahrmann, W., 1971a. Morphodynamics of the axolotl epidermis (*Siredon mexicanum* Shaw) under the influence of exogenously applied thyroxin: I. Epidermis of neotenic axolotl. Z. Mikrosk. Anat. Forsch. 83, 472–506.

Fahrmann, W., 1971b. Morphodynamics of the axolotl epidermis (*Siredon mexicanum* Shaw) under the influence of exogenously applied thyroxin: II. Epidermis during metamorphosis. Z. Mikrosk. Anat. Forsch. 83, 535–568.

Fahrmann, W., 1971c. Morphodynamics of the axolotl epidermis (*Siredon mexicanum* Shaw) under the influence of exogenously applied thyroxin: III. Epidermis of the metamorphosed axolotl. Z. Mikrosk. Anat. Forsch. 84, 1–25.

Fox, H., 1983. Changes in amphibian skin during larval development and metamorphosis. In: Balls, M., Bownes, M. (Eds.), Metamorphosis. British Society for Developmental Biology Symposium, vol. 8. Clarendon Press, Oxford, pp. 59–87.

Hayes, T.B., 1997. Steroid as potential modulators of thyroid hormone activity in anuran metamorphosis. Am. Zool. 37, 185–194.

Hayes, T.B., 2005. Welcome to the revolution: integrative biology and assessing the impact of endocrine disruptors on environmental and public health. Integr. Comp. Biol. 45, 321–329.

Helmreich, D.L., Parfitt, D.B., Lu, X.Y., Akil, L.H., Watson, S.J., 2005. Relation between the hypothalamic–pituitary–thyroid (HPT) axis and the hypothalamic–pituitary–adrenal (HPA) axis during repeated stress. Neuroendocrinology 81, 183–192.

Irizarry, R.A., Hobbs, B., Collin, F., Beazer-Barclay, Y.D., Antonellis, K.J., Scherf, U., Speed, T.P., 2003. Exploration, normalization, and summaries of high density oligonucleotide array probe level data. Biostatistics 4, 249–264.

Ishida, Y., Suzuki, K., Utoh, R., Obara, Y., Yoshizato, K., 2003. Molecular identification of the skin transformation center of anuran larval skin using genes of *Rana* adult keratin (RAK) and SPARC as probes. Dev. Growth Differ. 45, 515–526.

Kelly, D.E., 1966. Fine structure and function of amphibian epidermal Leydig cells. Anat. Rec. 154, 367.

Kester, M.H., Martinez de Mena, R., Obregon, M.J., et al., 2004. Iodothyronine levels in the human developing brain: major regulatory roles of iodothyronine deiodinases in different regions. J. Clin. Endocrinol. Metab. 89, 3117–3128.

Kinoshita, T., Sasaki, R., 1994. Adult precursor cells in the tail epidermis of *Xenopus* tadpoles. Histochemistry 101, 391–396.

Kitamura, S., Kato, T., Lida, M., Jinno, N., Suzuki, T., Ohta, S., Fujimoto, N., Hanada, H., Kashiwagi, K., Kashiwagi, A., 2005. Anti-thyroid hormonal activity of tetrabromobisphenol A, a flame retardant, and related compounds: affinity to the mammalian thyroid hormone receptor, and effect on tadpole metamorphosis. Life Sci. 76, 1589–1601.

Kuhn, E.R., De-Groef, B., Van-der-Geyten, S., Darras, V.M., 2005. Corticotropin-releasing hormone-mediated metamorphosis in the neotenic axolotl *Ambystoma mexicanum*: synergistic involvement of thyroxine and corticoids on brain type II deiodinase. Gen. Comp. Endocrinol. 143, 75–81.

Larsson, M., Pettersson, T., Carlström, A., 1985. Thyroid hormone binding in serum of 15 vertebrate species: isolation of thyroxine-binding globulin and pre-albumin analogs. Gen. Comp. Endocrinol. 58, 360–375.

Lazar, M.A., 1993. Thyroid hormone receptors: multiple forms, multiple possibilities. Endocr. Rev. 14, 184–193.

Mathisen, P.M., Miller, L., 1987. Thyroid hormone induction of keratin genes: a two-step activation of gene expression during development. Genes Dev. 1, 1107–1117.

Ohumura, H., Wakahara, M., 1998. Transformation of skin from larval to adult types in normally metamorphosing and metamorphosis-arrested salamander, *Hynobius retardatus*. Differentiation 63, 237–246.

Opitz, R., Braunbeck, T., Bögi, C., Pickford, D.B., Nentwig, G., Oehlmann, J., Tooi, O., Lutz, I., Kloas, K., 2005. Description and initial evaluation of a Xenopus Metamorphosis Assay (XEMA) for detection of thyroid system-disrupting activities of environmental compounds. Environ. Toxicol. Chem. 24, 653–664.

Power, D.M., Elias, N.P., Richardson, S.J., Mendes, J., Soares, C.M., Santos, C. R.A., 2000. Evolution of the thyroid hormone-binding protein, transthyretin. Gen. Comp. Endocrinol. 119, 241–255.

Putta, S., Smith, J.J., Walker, J.A., Rondet, M., Weisrock, D.W., Monaghan, J. R., Kump, D.K., King, D.C., Maness, N.J., Habermann, B., Tanaka, E., Bryant, S.V., Gardiner, D.M., Parichy, D.M., Voss, S.R., 2004. From biomedicine to natural history research: expressed sequence tag resources for ambystomatid salamanders. BMC Genomics 5, 54.

Reeder, A.L., Ruiz, M.O., Pessier, A., Brown, L.E., Levengood, J.M., Phillips, C.A., Wheeler, M.B., Warner, R.E., Beasley, V.R., 2005. Intersexuality and the cricket frog decline: historic and geographic trends. Environ. Health Perspect. 113, 261–265.

Reeves, O.R., 1975. Adult amphibian epidermal proteins: biochemical characterization and developmental appearance. J. Embryol. Exp. Morphol. 34, 55–73.

Reiner, A., Yekutieli, D., Benjamini, Y., 2003. Identifying differentially expressed genes using false discovery rate controlling procedures. Bioinformatics 19, 368–375.

Rozen, S., Skaletsky, H., 2000. Primer3 on the WWW for general users and for biologist programmers. Methods Mol. Biol. 132, 365–386.

Schreiber, A.M., Brown, D.D., 2002. Tadpole skin dies autonomously in response to thyroid hormone at metamorphosis. Proc. Natl. Acad. Sci. U. S. A. 100, 1769–1774.

Shimizu-Nishikawa, K., Miller, L., 1992. Hormonal regulation of adult type keratin gene expression in larval epidermal cells of the frog *Xenopus laevis*. Differentiation 49, 77–83.

Semlitsch, R.D., Scott, D.G., Pechmann, J.H.K., 1988. Time and size at metamorphosis related to adult fitness in *Ambystoma talpoideum*. Ecology 69, 184–192.

Shi, Y.-B., 2000. Amphibian Metamorphosis: From Morphology to Molecular Biology. Wiley-Liss Press, New York.

Smith, J.J., Putta, S., Walker, J.A., Kump, D.K., Samuels, A.K., Monaghan, J. R., Weisrock, D.W., Staben, C., Voss, S.R., 2005. Sal-site: integrating new and existing ambystomatid salamander research and informational resources. BMC Genomics 6, 181.

St. Germain, Galton, V.A., 1997. The deiodinase family of selanoproteins. Thyroid 7, 655–658.

Sturn, A. 2000. Cluster analysis for large scale gene expression studies. Master's Thesis: Institute for Biomedical Engineering, Graz University of Technology, Graz, Austria.

Sturn, A., Quackenbush, J., Trajanoski, Z., 2002. Genesis: cluster analysis of microarray data. Bioinformatics 18, 207–208.

Suzuki, K., Utoh, R., Kotani, K., Obara, M., Yoshizato, K., 2002. Lineage of anuran epidermal basal cells and their differentiation potential in relation to metamorphic skin remodeling. Dev. Growth Differ. 44, 225–238.

Tata, J.R., 1993. Gene expression during metamorphosis: an ideal model for post-embryonic development. BioEssays 15, 239–248.

Turque, N., Palmier, K., Le Mevel, S., Alliot, C., Demeneix, B.A., 2005. A rapid, physiologic protocol for testing transcriptional effects of thyroid-disrupting agents in premetamorphic *Xenopus* tadpoles. Environ. Health Perspect. 3, 1588–1593.

Voss, S.R., Smith, J.J., 2005. Evolution of salamander life cycles: a major effect QTL contributes to both continuous and discrete variation for metamorphic timing. Genetics 170, 181–275.

Watanabe, Y., Kobayaski, H., Suzuki, K., Kotani, K., Yoshizato, K., 2001. New epidermal keratin genes from *Xenopus laevis*: hormonal and regional regulation of their expression during anuran skin metamorphosis. Biochim. Biophys. Acta 1517, 339–350.

Wilbur, H.M., 1996. Multistage life cycles. In: Rhodes, O.E., Chesser, R.K., Smith, M.H. (Eds.), Population Dynamics in Ecological Space and Time. University of Chicago Press, Chicago, pp. 75–108.

Wu, H., Churchill, G.A., 2005. J/MAANOVA User Manual. http://www.jax.org/staff/churchill/labsite/software/Jmaanova/index.html.

Zhang, F., Degitz, S.J., Holcombe, G.W., Kosian, P.A., Tietge, J., Veldoen, N., Helbing, C.C., 2006. Evaluation of gene expression endpoints in the context of a *Xenopus laevis* metamorphosis-based bioassay to detect thyroid hormone disruptors. Aquat. Toxicol. 76, 24–36.

Zoeller, R.T., 2004. Editorial: local control of the timing of thyroid hormone action in the developing human brain. J. Clin. Endocrinol. Metab. 89, 3114–3116.